Food and Chemical Toxicology 126 (2019) 169–177

Contents lists available at ScienceDirect

Food and Chemical Toxicology

journal homepage: www.elsevier.com/locate/foodchemtox

The toxicity of multi-walled carbon nanotubes (MWCNTs) to human endothelial cells: The influence of diameters of MWCNTs

Xuqi Zhao[a,b,1], Shiwei Chang[a,b,1], Jimin Long[b], Juan Li[b], Xianqiang Li[a,**], Yi Cao[a,b,*]

[a] College of Animal Science, Key Laboratory of Tarim Animal Husbandry Science and Technology of Xinjiang Production and Construction Corps, Tarim University, Xinjiang, People's Republic of China

[b] Key Laboratory of Environment-Friendly Chemistry and Application of Ministry of Education, Laboratory of Biochemistry, College of Chemistry, Xiangtan University, Xiangtan, 411105, People's Republic of China

ARTICLE INFO

Keywords:
Multi-walled carbon nanotubes (MWCNTs)
Human umbilical vein endothelial cells (HUVECs)
Autophagy
ER stress
Toxicity

ABSTRACT

The biological applications of multi-walled carbon nanotubes (MWCNTs) may lead to their exposure to human blood vessels, but the influence of their physicochemical properties on toxicity to endothelial cells is incompletely known. Here, human umbilical vein endothelial cells (HUVECs) were exposed to three commercially available MWCNTs, namely XFM4, XFM22, and XFM34 (diameters XFM4 < XFM22 < XFM34), to understand the possible role of their diameter on toxicity. Based on the same mass concentration, XFM4 induced significantly higher level of cytotoxicity than the other two MWCNTs, and HUVECs internalized more XFM4. Cytokine release, monocyte adhesion, and intracellular reactive oxygen species levels were significantly induced only after XFM4 treatment. The exposure to XFM4 significantly reduced the expression of autophagic genes autophagy-related 7 (*ATG7*), autophagy-related 12 (*ATG12*), and beclin 1 (*BECN1*) and increased the expression of endoplasmic reticulum (ER) stress genes DNA damage inducible transcript 3 (*DDIT3*) and X-box binding protein 1 spliced (*XBP-1s*). Moreover, the modulation of autophagy-ER stress by chemicals resulted in a significant increase in the cytotoxicity of XFM4 but had minimal impact on the cytotoxicity of XFM34. These data indicate that the diameter of MWCNTs may influence their toxicity to HUVECs, probably through autophagy dysfunction and ER stress.

1. Introduction

Multi-walled carbon nanotubes (MWCNTs) are nanomaterials (NMs) with fiber-like structures. Their unique properties have been exploited for the development of several commercial products, including electronics, automotive, and appliances (Vance et al., 2015). MWCNTs have been recently explored as nanoplatforms for biomedical applications. For instance, MWCNTs as nanocarriers are suitable for the delivery of anticancer drugs, owing to their ability to load high amounts of hydrophobic anticancer molecules (Saleem et al., 2018). Functionalized MWCNTs hold great promises as novel anti-bacterial agents against multidrug-resistant bacterial infections (Mocan et al., 2017). Incorporation of MWCNTs into scaffolds may improve the functionality of cardiomyocytes, suggestive of their applications in myocardial tissue regeneration (Gorain et al., 2018). However, their potential toxicity and mechanism of action should be evaluated to ensure safe use. In particular, the toxicity of MWCNTs to human endothelial cells, the surface cells covering blood vessels, should be carefully evaluated because the use of MWCNTs in biomedicine may increase the direct contact between NMs and blood vessels. However, nanomedicinal studies often ignore the importance of investigating the adverse effects of NMs to human endothelial cells, since blood vessels are seldom the targets in nanomedicine (Cao et al., 2017a; Setyawati et al., 2015).

In general, the toxicity of MWCNTs is largely dependent on their

Abbreviations: ATG7, autophagy related 7; ATG12, autophagy related 12; Baf A1, bafilomycin A1; BECN1, beclin 1; CCK-8, cell counting kit-8; DDIT3, DNA damage inducible transcript 3; HSPA5, (heat shock protein family A (Hsp70) member 5; HUVEC, human umbilical vein endothelial cell; IL-6, interleukin-6; MWCNT, multi-walled carbon nanotube; NC, nitrocellulose; NM, nanomaterial; PDI, polydispersity index; RAPA, rapamycin; ROS, reactive oxygen species; sVCAM-1, soluble vascular cell adhesion molecule-1; TEM, transmission electron microscope; TG, thapsigargin; XBP-1s, X-box binding protein 1 spliced

* Corresponding author. Key Laboratory of Environment-Friendly Chemistry and Application of Ministry of Education, Laboratory of Biochemistry, College of Chemistry, Xiangtan University, Xiangtan, 411105, People's Republic of China.

** Corresponding author.

E-mail addresses: lixianqiang89@sina.com (X. Li), caoyi39@126.com (Y. Cao).

[1] These two authors contributed equally to this work.

https://doi.org/10.1016/j.fct.2019.02.026
Received 17 January 2019; Received in revised form 15 February 2019; Accepted 18 February 2019
Available online 22 February 2019
0278-6915/

physicochemical properties, predominantly the length, diameter, and surface chemistry. Control over these parameters may be an effective strategy to reduce the adverse effects of MWCNTs (Li and Cao, 2018; Louro, 2018). How the physicochemical properties determine the toxicity of MWCNTs to endothelial cells is yet incompletely understood. Orecna et al. (2014) found that carboxylated MWCNTs, but not pristine MWCNTs, significantly induced cytotoxicity to human umbilical vein endothelial cells (HUVECs), suggestive of the role of surface chemistry in this effect. Zhao et al. (2014) showed that the presence of nitrogen in MWCNTs enhanced the cytocompatibility of MWCNTs with endothelial cells. We recently revealed the length-dependent toxicity of MWCNTs to HUVECs (Long et al., 2017). Further work is warranted to explore how the physicochemical properties of MWCNTs influence the toxicity to endothelial cells.

The effects of the physicochemical properties of MWCNTs on their signaling pathways also need to be evaluated. Recent studies have suggested that autophagy-endoplasmic reticulum (ER) stress may be involved in the toxicity of NMs. Autophagy is a process of self-degradation of cellular components, and studies have revealed that NM exposure may induce autophagy dysfunction (excessive or defective induction of autophagy) that is linked to the toxicity of NMs (Li and Ju, 2018; Ou et al., 2016). Several studies have demonstrated the emerging role of autophagy in mediating the toxic effects of MWCNTs (Cohignac et al., 2018; Orecna et al., 2014; Tsukahara et al., 2014; Zhao et al., 2018). As an adaptive response, ER stress is interconnected with autophagy dysfunction (Rashid et al., 2015; Smith and Wilkinson, 2017) and NMs may induce ER stress, leading to cell death (Cao et al., 2017b). The influence of MWCNTs on ER stress is less studied, but we and others have recently reported the ER stress-dependent toxicity in MWCNT-exposed HUVECs (Long et al., 2017), alveolar-endothelial co-culture (Chang et al., 2018), and *Caenorhabditis elegans* (Eom et al., 2015). How MWCNT-induced autophagy-ER stress response in HUVECs is influenced by the physicochemical properties of MWCNTs, however, remains unclear.

We have recently reported the length-dependent toxicity of MWCNTs to HUVECs that was associated with ER stress (Long et al., 2017). In this study, we investigated the diameter-dependent toxicity of MWCNTs to HUVECs via autophagy-ER stress pathway. Three types of MWCNTs with similar length but different diameters were used in this study. HUVECs were exposed to different concentrations of MWCNTs, and cytotoxicity was measured with cell counting kit-8 (CCK-8) assay. The internalization of MWCNTs into HUVECs was measured by both transmission electron microscopy (TEM) and light scatter analysis. The release of interleukin-6 (IL-6) and soluble vascular cell adhesion molecule-1 (sVCAM-1) as well as the adhesion of THP-1 monocytes to HUVECs were determined to confirm inflammatory responses. Intracellular reactive oxygen species (ROS) level was determined to evaluate oxidative stress. We measured these endpoints as they are closely related with the early development of atheroslerosis (Cao et al., 2017a), hence the results could provide systemic understanding about how the diameters of MWCNTs influence the toxicity of MWCNTs to vascular systems. The involvement of autophagy-ER stress was investigated with real-time reverse-transcription polymerase chain reaction (RT-PCR) to measure the expression of autophagic genes, namely autophagy-related 7 (*ATG7*; Gene ID 10,533), autophagy-related 12 (*ATG12*; Gene ID 9140), and beclin 1 (*BECN1*; Gene ID 8678), as well as typical ER stress genes, namely, DNA damage inducible transcript 3 (*DDIT3*; Gene ID 1649), X-box binding protein 1 spliced (*XBP-1s*), and heat shock protein family A [Hsp70] member 5 (*HSPA5*; Gene ID 3309). The protein levels of LC3-I and LC3-II, the biomarkers of autophagy, were also determined by western blot analysis.

2. Materials and methods

2.1. Cell culture

HUVECs at passage 1 were purchased from ScienCell Research Laboratories (Carlsbad, CA) and were cultured in supplemented endothelial medium following supplier's instructions. During the experiments, HUVECs were used at passages 3–6 to keep their best characteristics. THP-1 monocytes (purchased from the American Type Culture Collection, Manassas, VA, USA) were cultured in supplemented Roswell Park Memorial Institute (RPMI)-1640 medium (Gibco, NY, USA) and used within 2 months.

2.2. MWCNT characterization and preparation

MWCNTs with different diameters (code XFM4, XFM22, and XFM34) were purchased from Nanjing XFNANO Materials Tech Co., Ltd. The physicochemical properties, including purity, primary size, specific surface area, tap density, true density, and electric conductivity, were measured by the supplier and the information is summarized in Supplemental Table S1. In the present study, TEM (FEI TECNAI G20, Hillsboro, OR, USA) was used to investigate the morphology and structure of MWCNTs. The diameters of 20 randomly selected MWCNTs were determined with ImageJ (NIH) and the mean ± standard deviation (SD) was calculated.

To prepare the suspensions of MWCNTs, a stock solution of 1.28 mg/mL particles in Milli-Q water containing 2% fetal bovine serum (FBS) was prepared with continuous sonication (twice for 8 min with cooling on ice) using an ultrasonic processor FS-250N (20% amplitude; Shanghai Shengxi, Shanghai, China). The freshly prepared stock solution was diluted with cell culture medium to obtain the desired concentrations. To measure the hydrodynamic size and zeta potential distribution, 32 μg/mL of MWCNTs were prepared in Milli-Q water or medium and analyzed using Zetasizer nano ZS90 (Malvern, Amesbury, UK).

2.3. Cytotoxicity assays

The cytotoxicity of the samples was measured with CCK-8 assay using a commercial kit (Beyotime, Nantong, China). Briefly, 4×10^4 HUVECs/well were seeded in a 24-well plate. After cultivation for 2 days, the cells were incubated with fresh medium containing 0 (control), 4, 8, 16, 32, and 64 μg/mL MWCNTs. After exposure for 24 h, the cytotoxicity assay was performed according to the manufacturer's instructions (Beyotime, Nantong, China). The final products were evaluated using an enzyme-linked immunosorbent assay (ELISA) reader (Synergy HT, BioTek, Woburn, MA, USA). As we observed diameter-dependent cytotoxicity and autophagy-ER stress signaling alteration (see in results), we modulated autophagy-ER stress with chemicals to evaluate the possible role of autophagy-ER stress in MWCNT-mediated cytotoxicity. The cells were incubated with 200 nM thapsigargin (TG, ER stress activator; CST Cell Signaling Technology, Danvers, MA, USA), 100 nM bafilomycin A1 (Baf A1, autophagy inhibitor; CST Cell Signaling Technologies, USA), or 200 nM rapamycin (RAPA, autophagy activator; Vetec™ Sigma-Aldrich, USA) for 1 h. Cells incubated with medium for 1 h served as control. Following incubation, the old medium was replaced with fresh medium containing 64 μg/mL XFM4 and XFM34 for 24 h prior to CCK-8 assay as indicated above.

2.4. TEM study

For ultrastructural observation, cells were seeded at a density of 5×10^5 in a 60 mm diameter cell culture Petri dish and cultivated for 2 days. The cells were exposed to 64 μg/mL XFM4, XFM22, and XFM34 for 24 h. After exposure, the cells were rinsed and scratched using a cell scraper. After centrifugation, the cells were fixed with 2.5%

glutaraldehyde in phosphate-buffered saline (PBS) overnight, post-fixed with 1% osmium tetroxide (OsO_4) for 3 h, dehydrated in a graded series of ethanol, and embedded in epoxy resin (Epon 812). The samples were sectioned using an ultramicrotome at 70 nm thickness, placed on a carbon film supported by copper grids, stained with uranyl acetate and lead citrate, and observed under a transmission electron microscope (JEM-1230, JEOL Ltd., Tokyo, Japan) operated at 80 kV.

2.5. Light scatter analysis

The internalization of MWCNTs into HUVECs was further measured using light scatter analysis. Here HUVECs were cultured in 12-well plates at a density of 1×10^5 cells/well and grown for 2 days before exposure to 64 μg/mL XFM4, XFM22, and XFM34 for 24 h. HUVECs incubated with cell culture medium for 24 h were used as control. After exposure, the cells were removed from plates by using trypsin, and then analyzed by flow cytometry (BD LSRFortessa™, Franklin Lakes, NJ, USA). For each sample, 5000 events were analyzed.

2.6. Adhesion assay

The adhesion of THP-1 cells to HUVECs was measured using a fluorescent probe CellTracker™ green 5-chloromethylfluorescein diacetate (CMFDA; Invitrogen, Carlsbad, CA). Briefly, HUVECs were cultured in 96-well black plates at a density of 1×10^4 cells/well and grown for 2 days before exposure to various concentrations of MWCNTs (from 0 to 64 μg/mL) for 24 h. At the end of the exposure, THP-1 monocytes were labeled with 10 μM CellTracker™ green CMFDA, and 5×10^4 cells/well were incubated with the exposed HUVECs for another 1 h. The unbound THP-1 cells were washed away, and the green fluorescence from the adherent THP-1 cells was read at an excitation wavelength of 485 ± 20 nm and emission wavelength of 528 ± 20 nm with ELISA reader.

2.7. Intracellular ROS level

The level of intracellular ROS was measured using a general ROS indicator 2′,7′-dichlorodihydrofluorescein diacetate (DCFH-DA). Briefly, 1×10^4 HUVECs were seeded in each well of a 96-well black plate and exposed to various concentrations of MWCNTs. After exposure, the cells were rinsed once and incubated with 10 μM DCFH-DA (Sigma-Aldrich) in serum-free medium for 30 min. The cells were rinsed once and the fluorescence was read at an excitation wavelength of 485 ± 20 nm and emission wavelength of 528 ± 20 nm with ELISA reader.

2.8. Cytokine measurement by ELISA

Before CCK-8 assay, the supernatants from the cell culture were collected and stored at −20 °C. The concentrations of IL-6 and sVCAM-1 were determined with ELISA kits according to the manufacturer's instructions (NeoBioscience Technology Co., Ltd., Guangzhou, China). All the cytokines were detectable in each sample.

2.9. Real-time RT-PCR

The mRNA levels of *ATG7*, *ATG12*, *BECN1*, *DDIT-3*, *XBP-1s*, *HSPA5*, and glyceraldehyde-3-phosphate dehydrogenase (*GAPDH*) were determined with real-time quantitative RT-PCR. Briefly, 2×10^5 HUVECs were seeded in each well of a six-well plate and cultured for 2 days. The cells were incubated with 0 (control) and 64 μg/mL MWCNTs for 24 h. After exposure, the cells were rinsed once with Hank's solution, and the total mRNA was extracted using TRI Reagent® following manufacturer's instructions (Sigma-Aldrich, USA). The cDNA was synthesized by using HiFiScript cDNA Synthesis Kit following manufacturer's instructions (Cwbiotech, Beijing, China). Real-time quantitative PCR was performed using UltraSYBR Mixture (Cwbiotech, Beijing, China) on PikoReal™ qPCR system (Thermo-Fisher, USA). The primers for each gene are summarized in Supplemental Table S2. The mRNA levels were expressed as the ratio of target genes and internal control gene.

2.10. Western blot analysis

The protein levels of LC3-I, LC3-II, and β-actin (internal control) were determined with western blotting. Briefly, 2×10^5 HUVECs were seeded in each well of a six-well plate and cultured for 2 days before exposure to 0 (control) and 64 μg/mL MWCNTs for 24 h. After exposure, the cells were rinsed twice with Hank's solution, and treated with radioimmunoprecipitation assay (RIPA) lysis buffer in the presence of protease inhibitor cocktail and PhosStop™ phosphatase inhibitor (Roche Diagnostics). The samples were placed on ice for 10 min, and the supernatants were collected by centrifugation for 15 min at 12,000 rpm and 4 °C. The protein concentrations were measured with bicinchoninic acid (BCA) method, and each sample (50 μg protein) was mixed with a loading buffer and resolved by sodium dodecyl sulfate polyacrylamide gel electrophoresis (SDS-PAGE). The samples were transferred onto a nitrocellulose (NC) membrane, blocked with non-fat milk for 1.5 h at room temperature, and incubated overnight at 4 °C with primary antibody (1:1000 LC3, CST Cell Signaling Technologies, USA; 1:5000 β-actin antibody, Proteintech, USA). The blots were washed with 0.1% w/v Tween-PBS and incubated with 1:5000 horseradish peroxidase (HRP) goat anti-rabbit IgG (Proteintech, USA) for 1.5 h. The blots were detected with SuperECL Plus chemiluminescence (Thermo pierce, USA). The experiment was repeated for three times, and the density of each band was determined by using ImageJ (National Institutes of Health). The unedited western blot images are shown in Supplementary Fig. S1.

2.11. Statistics

The data were expressed as mean ± standard deviation of mean (SD) of three independent experiments (n = 3 for each). Two-way analysis of variance (ANOVA) followed by Tukey's honestly significant difference (HSD) test was used to compare the difference in R 3.3.3. A value of $p < 0.05$ was considered as statistically significant.

3. Results

3.1. Characteristics of MWCNTs

According to the suppliers, XFM4, XFM22, and XFM34 are MWCNTs with similar lengths (0.5–2 μm) but different diameters in the following order: XFM4 < XFM22 < XFM34 (Supplemental Table S1). This observation was supported by TEM images (Fig. 1); the average diameters of XFM4, XFM22, and XFM34 were calculated as 10.33 ± 3.50, 21.55 ± 5.66, and 38.80 ± 13.07 nm, respectively. As MWCNTs formed agglomerates/aggregates, their lengths were not measured. The distribution of the hydrodynamic size and zeta potential of XFM4, XFM22, and XFM34 is shown in Supplemental Fig. S2. XFM4 appeared to have a higher hydrodynamic size, lower absolute zeta potential in water, and larger polydispersity index (PDI) than XFM22 and XFM34 (Table 1).

3.2. Cytotoxicity of MWCNTs

The results of CCK-8 assay shown in Fig. 2 indicated a dose-dependent decrease in the viability of HUVECs after exposure to XFM4 and XFM22 ($p < 0.01$) but not XFM34 ($p > 0.05$). A statistically significant decrease in cellular viability was observed after exposure to 16, 32, and 64 μg/mL of XFM4 ($p < 0.01$) or 64 μg/mL of XFM22 ($p < 0.01$). Moreover, the viability of the cells exposed to 32 μg/mL of XFM4 was significantly lower than that of cells exposed to 32 μg/mL of

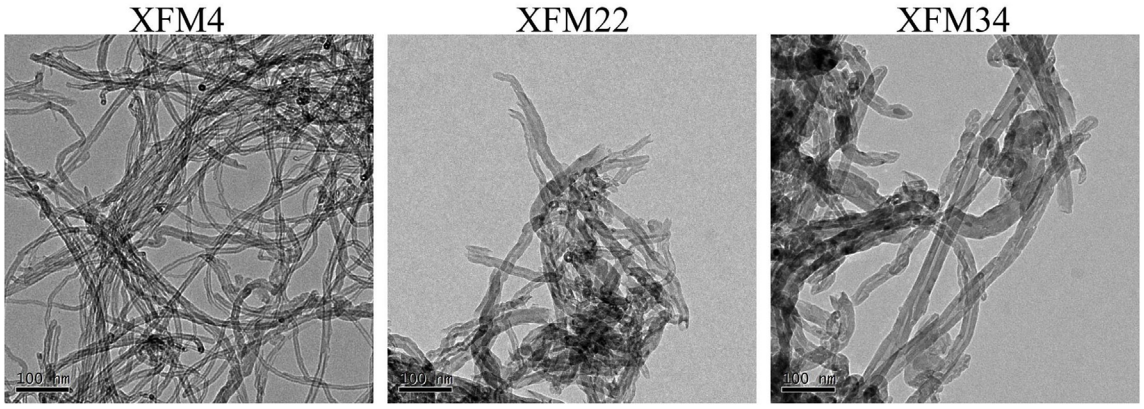

Fig. 1. Representative TEM images of XFM4 (left), XFM22 (center), and XFM34 (right).

Table 1
The average hydrodynamic size, zeta potential, and PDI of XFM4, XFM22, and XFM34 in water and medium.

Code	Suspension	Hydrodynamic size (nm)	Zeta potential (mV)	PDI
XFM4	Water	292.00 ± 3.97	−8.70 ± 0.83	0.504 ± 0.062
	Medium	304.90 ± 4.49	−9.48 ± 0.33	0.497 ± 0.042
XFM22	Water	183.23 ± 3.97	−21.47 ± 0.25	0.232 ± 0.008
	Medium	205.90 ± 0.44	−8.02 ± 0.35	0.228 ± 0.010
XFM34	Water	179.13 ± 1.33	−25.10 ± 0.40	0.230 ± 0.023
	Medium	205.90 ± 0.44	−8.57 ± 0.55	0.245 ± 0.014

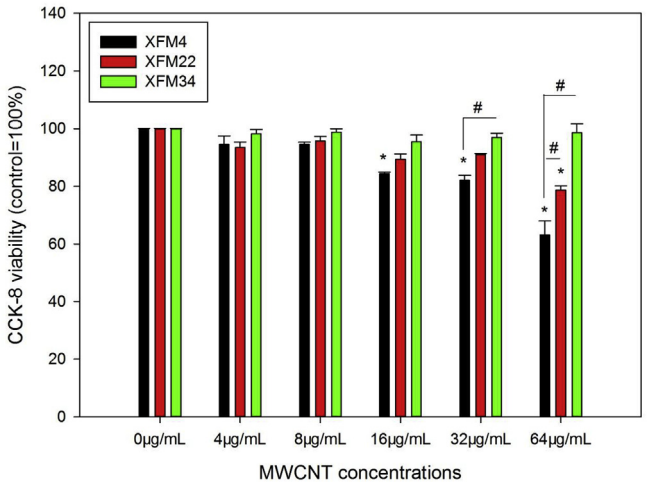

Fig. 2. Cytotoxicity of XFM4, XFM22, and XFM34 to HUVECs, as assessed with CCK-8 assay. HUVECs were exposed to various concentrations of MWCNTs for 24 h, and CCK-8 assay was performed to evaluate cytotoxicity. *, $p < 0.05$ as compared with control. #, $p < 0.05$.

XFM34 ($p < 0.01$). The viability of the cells was similarly lower after exposure to 64 μg/mL of XFM4 than 64 μg/mL of XFM22 and XFM34 ($p < 0.01$).

3.3. Ultrastructural changes in HUVECs and internalization of MWCNTs

The representative TEM images shown in Fig. 3 indicated no obvious changes in the ultrastructure of HUVECs after MWCNT exposure as compared with control. Internalization was observed for all types of MWCNTs, but maximum internalization was observed for XFM4. This observation was further confirmed by light scatter analysis, as HUVECs exposed to XFM4 showed the largest change in side-scattered light (SSC; Supplemental Fig. S3B).

3.4. The release of cytokines

The release of IL-6 (Fig. 4A) and sVCAM-1 (Fig. 4B) significantly increased after the exposure of the cells to 64 μg/mL of XFM4 ($p < 0.01$) but not XFM22 or XFM34 ($p > 0.05$). Moreover, the level of cytokine released was significantly higher for the cells treated with 64 μg/mL of XFM4 than for those treated with 64 μg/mL of XFM22 or XFM34 ($p < 0.01$).

3.5. Adhesion of THP-1 monocytes onto HUVECs

As shown in Fig. 5, the adhesion of THP-1 monocytes onto HUVECs was significantly induced only after treatment with 64 μg/mL of XFM4 ($p < 0.05$), and the effect was significantly higher than that observed following XFM22 and XFM34 treatment at the same concentration ($p < 0.05$).

3.6. Intracellular ROS

Intracellular ROS level significantly increased after exposure to 64 μg/mL of XFM4 ($p < 0.01$). The level of ROS induced by 64 μg/mL of XFM4 was significantly higher than that induced by 64 μg/mL of XFM22 and XFM34 ($p < 0.05$; Fig. 6).

3.7. Autophagy-ER stress genes and proteins

The changes in the expression patterns of autophagic genes and proteins are shown in Fig. 7. The expression of *ATG7* significantly decreased after treatment of cells with 64 μg/mL XFM4 and XFM22 ($p < 0.01$); *ATG7* expression was significantly lower in the cells treated with 64 μg/mL of XFM4 and XFM22 than in those treated with 64 μg/mL of XFM34 ($p < 0.01$; Fig. 7A). The expression of *ATG12* significantly decreased in the cells treated with all types of MWCNTs ($p < 0.01$), but the treatment with XFM4 significantly lowered the expression of *ATG12* as compared with XFM22 and XFM34 treatment ($p < 0.01$; Fig. 7B). For *BECN1* (Fig. 7C), the expression significantly decreased in XFM4-and XFM22-exposed cells ($p < 0.01$), and the mRNA levels of *BECN1* followed an order of XFM34 > XFM22 > XFM4 ($p < 0.01$). As shown in Fig. 7D, the exposure of cells to XFM4 led to a significant increase in LC3-II/LC3-I ratio ($p < 0.01$), whereas XFM22 significantly decreased LC3-II/LC3-I ratio. Moreover, the cells exposed to XFM4 had a significantly higher LC3-II/LC3-I ratio compared with the cells exposed to XFM22 or XFM34 ($p < 0.01$).

The evaluation of the expression of ER stress genes showed that *DDIT3* (Fig. 8A) and *XBP-1s* (Fig. 8B) expression levels after XFM4 treatment were significantly higher ($p < 0.01$) than those observed after XFM22 and XFM34 treatment ($p < 0.01$). The expression of *HSPA5* (Fig. 8C) significantly decreased after XFM4 and XFM22

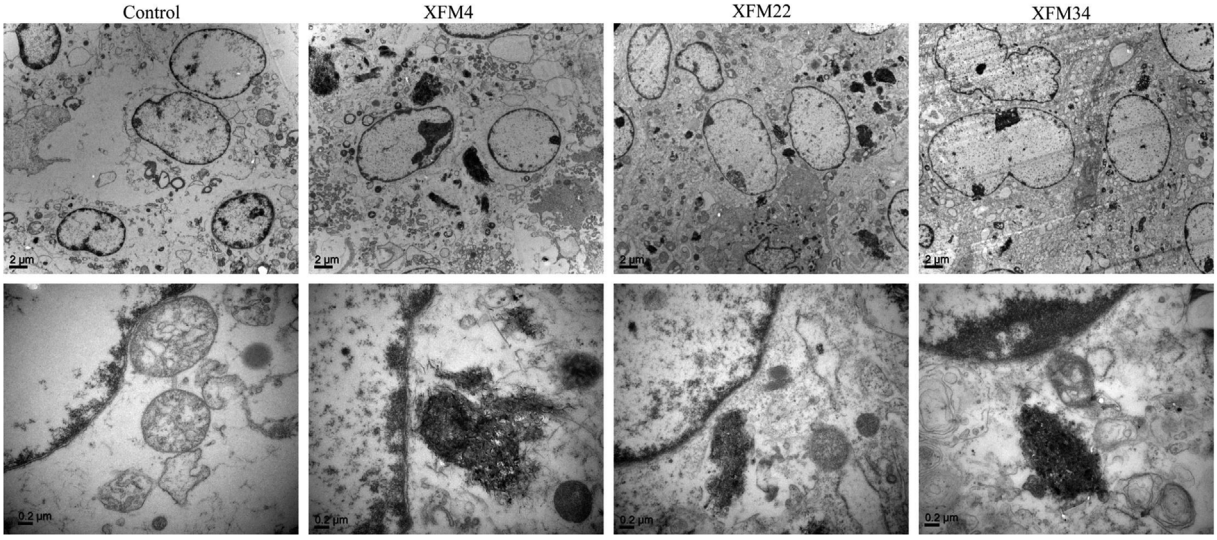

Fig. 3. Representative TEM images of HUVECs. HUVECs were incubated with medium (control), 64 μg/mL of XFM4, XFM22, and XFM34 for 24 h, and TEM was used to visualize the ultrastructural changes in cells as well as the internalization of MWCNTs.

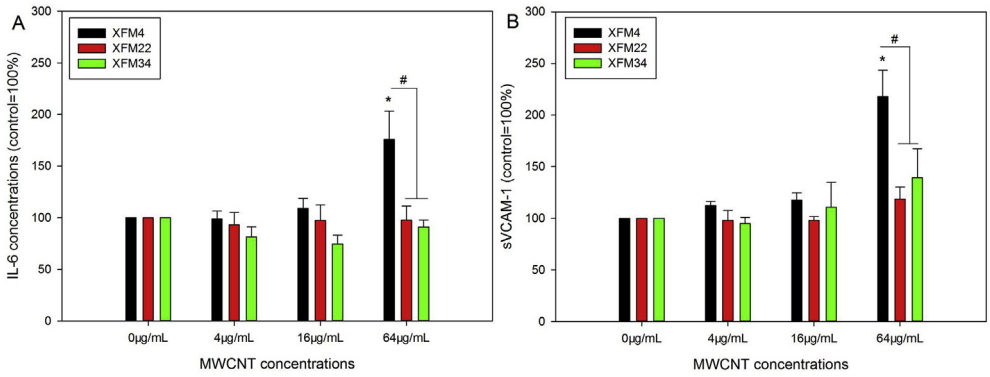

Fig. 4. Release of IL-6 (Fig. 4A) and sVCAM-1 (Fig. 4B). The supernatants from MWCNT-exposed cells were collected before CCK-8 assay, and the concentrations of cytokines were determined with ELISA. *, $p < 0.05$ as compared with control. #, $p < 0.05$.

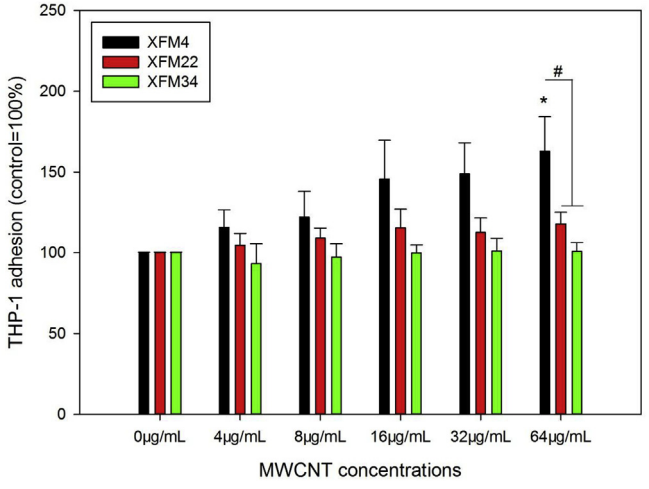

Fig. 5. Adhesion of THP-1 monocytes onto HUVECs. HUVECs were exposed to various concentrations of MWCNTs for 24 h, and the adhesion of THP-1 monocytes onto HUVECs was determined using a fluorescent probe CellTracker™ green. *, $p < 0.05$ as compared with control. #, $p < 0.05$. (For interpretation of the references to colour in this figure legend, the reader is referred to the Web version of this article.)

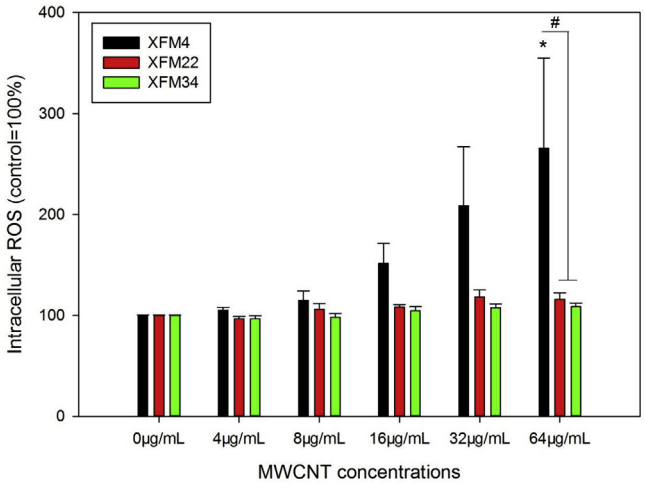

Fig. 6. Production of intracellular ROS. HUVECs were exposed to various concentrations of MWCNTs for 24 h, and intracellular ROS level was determined with a fluorescent probe DCFH-DA. *, $p < 0.05$ as compared with control. #, $p < 0.05$.

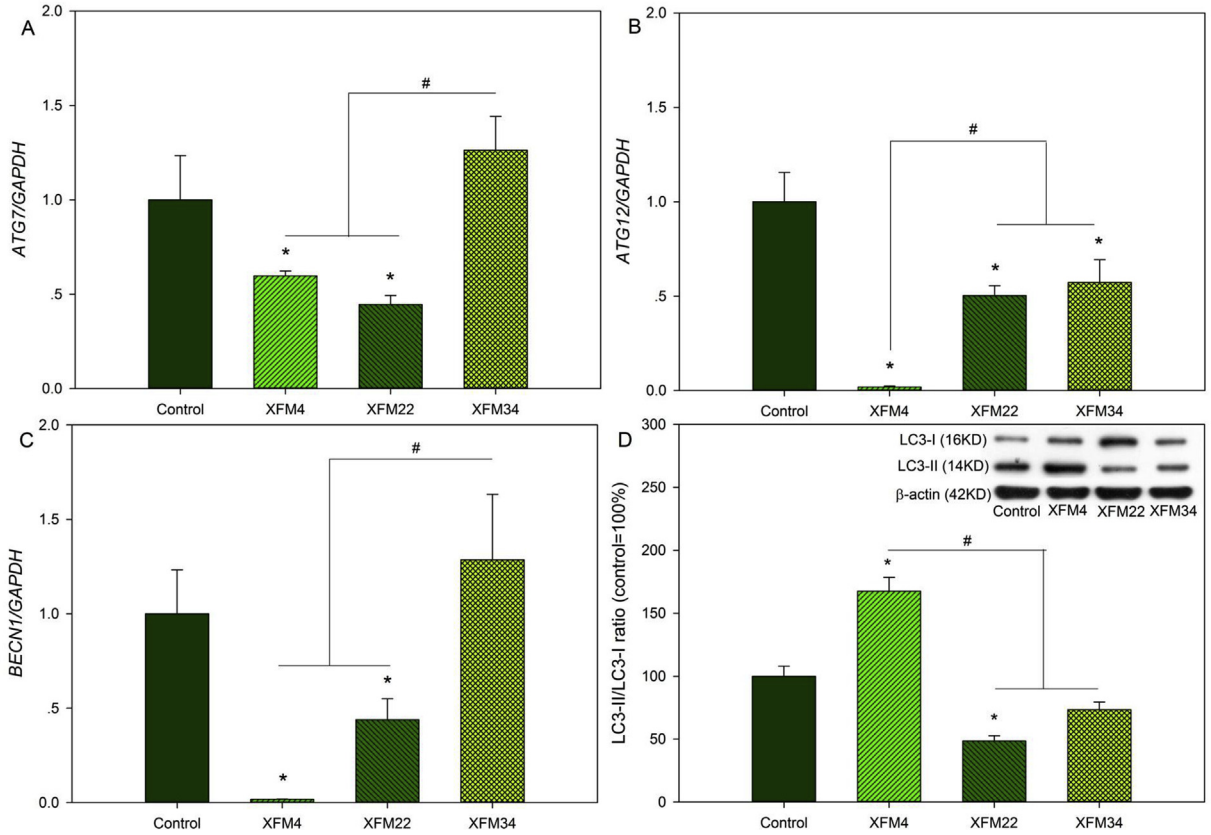

Fig. 7. Changes in the mRNA levels of autophagic genes *ATG7* (7A), *ATG12* (7B), and *BECN1* (7C) as well as protein levels of LC3-I, LC3-II, and β-actin (7D). HUVECs were exposed to 64 μg/mL of XFM4, XFM22, and XFM34 for 24 h. After exposure, real-time RT-PCR was performed to determine the mRNA levels. Western blot analysis was carried out to measure protein levels. *, $p < 0.05$ as compared with control. #, $p < 0.05$.

treatment ($p < 0.01$) but was unaltered after XFM34 treatment ($p > 0.05$). The mRNA levels of *HSPA5* followed an order of XFM34 > XFM22 > XFM4 ($p < 0.01$).

3.8. Changes in the cytotoxicity of MWCNTs in response to autophagy-ER stress modulators

The viability of HUVECs was significantly decreased following pre-incubation with TG and Baf A1 ($p < 0.01$) but not RAPA ($p > 0.05$; Supplemental Fig. S4). Pre-treatment of cells with TG, Baf A1, and RAPA resulted in a significant increase in the cytotoxicity of XFM4 to HUVECs ($p < 0.01$; Fig. 9A). In contrast, the cytotoxicity of XFM34 was only significantly enhanced after pre-treatment with Baf A1 ($p < 0.1$; Fig. 9B).

4. Discussion

The contribution of diameter to MWCNT-induced toxicity to vascular systems is not fully known. Here we investigated the diameter-dependent toxicity of MWCNTs to an *in vitro* model of endothelial cells (HUVECs) and the possible involvement of autophagy-ER stress underlying this effect. Three commercially available MWCNTs with different diameters were used and the difference in their diameters was verified with TEM (Fig. 1). The diameters followed an order of XFM4 < XFM22 < XFM34. The hydrodynamic size, zeta potential, and PDI of XFM4 were different from those of XFM22 and XFM34 at same mass concentration (Table 1), indicative of the different aggregate/agglomerate status of MWCNTs in suspension (Bhattacharjee, 2016). The differences in the diameters may have contributed to the different degrees of internalization of MWCNTs into HUVECs, as evident from TEM images (Fig. 3) and light scatter analysis (Supplemental

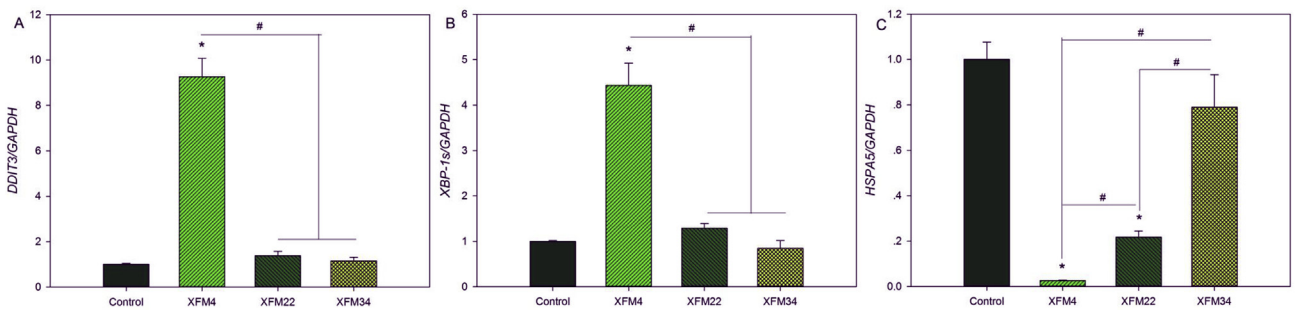

Fig. 8. Expression of ER stress genes *DDIT3* (8A), *XBP-1s* (8B), and *HSPA5* (8C). HUVECs were exposed to 64 μg/mL of XFM4, XFM22, and XFM34 for 24 h, and real-time RT-PCR was performed to measure the expression levels of ER stress genes. *, $p < 0.05$ as compared with control. #, $p < 0.05$.

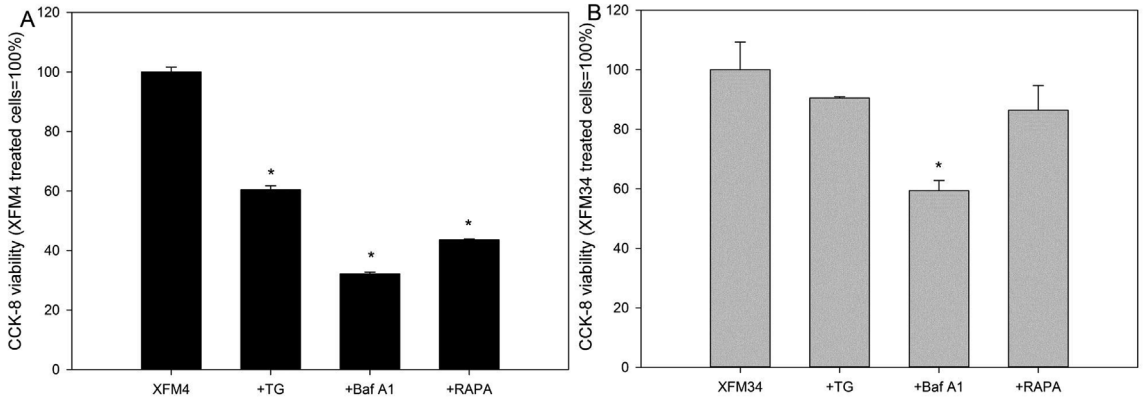

Fig. 9. Influence of autophagy-ER stress modulators on the cytotoxicity of XFM4 (9A) and XFM34 (9B). HUVECs were incubated with medium (control), 200 nM TG, 100 nM Baf A1, and 200 nM RAPA for 1 h prior to 24 h exposure to 64 μg/mL of XFM4 and XFM34. CCK-8 assay was performed to evaluate cytotoxicity. *, $p < 0.01$ as compared with control (cells exposed to MWCNTs only).

Fig. S3B), because the physicochemical properties may influence the interaction between MWCNTs and cells (Raffa et al., 2010). However, the exact influence of diameters on the internalization of MWCNTs into endothelial cells may need further studies.

The results of the CCK-8 assay revealed the gradual decrease in cytotoxicity with an increase in the diameters of MWCNTs at same mass concentration (Fig. 2). At present, the effect of diameter on the toxicity of MWCNTs is incompletely known. Yang et al. (2017) found that MWCNTs with smaller diameters generally displayed stronger toxicity toward bacteria. In contrast, Poulsen et al. (2016) showed that the inhalational exposure to MWCNTs with large diameters or low surface area resulted in high genotoxicity in mice. Therefore, the exact influence of the diameter of MWCNTs on toxicity may be dependent on the models and endpoints analyzed. We have found that the toxicity of MWCNTs to HUVECs is length-dependent (Long et al., 2017). The results of the present study suggest that the toxicity may be diameter-dependent compared on a mass basis. To the best of our knowledge, this is the first study to investigate the diameter-dependent toxicity to endothelial cells, and the results indicate that the diameter should be considered as an important parameter during the design of safe MWCNTs for human use.

Exposure to carbon nanotubes may promote inflammatory responses and oxidative stress, which could be linked to the development of chronic vascular diseases such as atherosclerosis (Moller et al., 2016; Rezaee et al., 2018). In the present study, we showed that the direct contact with MWCNTs promoted cytokine release (Fig. 4), monocyte adhesion (Fig. 5), and intracellular ROS production (Fig. 6), consistent with the previous reports showing that carbon nanotubes could promote the activation of endothelial cells *in vitro* (Bhattacharjee, 2016; Cao et al., 2014; Long et al., 2017; Lu et al., 2018; Suzuki et al., 2016). Compared with previous studies, our study further showed that MWCNT-induced endothelial activation *in vitro* could be dependent on the diameter of MWCNTs, as these responses were only observed in HUVECs exposed to MWCNTs with the smallest diameter (XFM4).

To investigate the mechanism associated with the diameter-dependent toxicity, we investigated the possible role of autophagy and ER stress. Previous studies have shown that MWCNTs could activate autophagy, as evident from the increased LC3-II/LC3-I ratio (Cohignac et al., 2018; Gao et al., 2015; Hamilton et al., 2018; Orecna et al., 2014; Wu et al., 2014). This effect was also observed in XFM4-exposed HUVECs (Fig. 7D). The induction of autophagy could be an adaptive response to MWCNT exposure, as the autophagy machinery may degrade the internalized NMs as well as the damaged organelles and proteins (Li and Ju, 2018; Ou et al., 2016). However, the expression of autophagy regulators *ATG7*, *ATG12*, and *BECN1* was downregulated particularly after exposure to XFM4 (Fig. 7A–C). MWCNT-induced autophagy was thought to be associated with autophagy blockade, and stimulation of autophagic flux that enhanced the extracellular release of NMs could be cytoprotective to MWCNT exposure (Cohignac et al., 2018; Orecna et al., 2014). Therefore, the downregulation of autophagy genes may result in the impairment in the ability of HUVECs to degrade MWCNTs, and this may serve as the mechanisms underlying MWCNT-induced cytotoxicity. This phenomenon was observed after that the pre-treatment of cells with Baf A1, an autophagy inhibitor, significantly augmented the toxicity of XFM4 and XFM34 to HUVECs (Fig. 9). However, the pre-treatment of cells with RAPA, an autophagy activator, also significantly enhanced the toxicity of XFM4 (Fig. 9A). This observation could be explained by the dual role of autophagy in cytotoxicity; excessive induction of autophagy and accumulation of autophagosomes may lead to autophagic cell death (Li and Ju, 2018; Ou et al., 2016). Nevertheless, both activation and inhibition of autophagy by chemicals could enhance the cytotoxicity of the thin MWCNTs to HUVECs, indicative of the role of autophagy dysfunction in diameter-dependent toxicity of MWCNTs.

ER stress is interconnected with autophagy dysfunction (Rashid et al., 2015; Smith and Wilkinson, 2017). As we observed autophagy dysfunction, we addressed whether MWCNT could influence ER stress. The results showed that ER stress biomarkers, *DDIT3* and *XBP-1s*, were significantly elevated only after the exposure of the cells to XFM4 (Fig. 8). The induction of ER stress by MWCNT exposure is consistent with our previous observations using HUVECs (Long et al., 2017) and alveolar-endothelial co-culture (Chang et al., 2018). A previous study reported activation of ER stress and cell death pathway following single-walled carbon nanotube exposure, suggesting that ER stress may be responsible for the toxicity of carbon nanotubes (Park et al., 2014). Here, we further showed that MWCNT-induced ER stress is diameter-dependent, as the induction of *DDIT3* and *XBP-1s* was only observed in cells treated with XFM4 but not XFM22 or XFM24 (Fig. 8). In addition, the role of ER stress in MWCNT-induced cytotoxicity could be evidenced, as the pre-treatment of cells with TG significantly promoted the cytotoxicity of XFM4 to MWCNTs (Fig. 9A). Although TG and Baf A1 also significantly induced cytotoxicity (Supplemental Fig. S4), we argue that our data could indicate that HUVECs exposed to XFM4 were more sensitive to the changes of autophagy and ER stress compared with the cells exposed to XFM34.

In this study, we observed most of the adverse effects at the concentration of 64 μg/mL, although XFM4 also significantly induced cytotoxicity at the concentrations larger than 16 μg/mL (Fig. 2). The concentrations used in this study (4–64 μg/mL) were comparable to those used in previous studies with similar purposes (Cao et al., 2017a). In nanomedicine, Kafa et al. and Wang et al. injected mice intravenously with 50 μg MWCNTs as nanocarriers to cross blood-brain barriers (Kafa et al., 2016; Wang et al., 2016). The concentration of 50 μg MWCNT/mouse equals to 25 μg/mL MWCNTs in blood, assuming

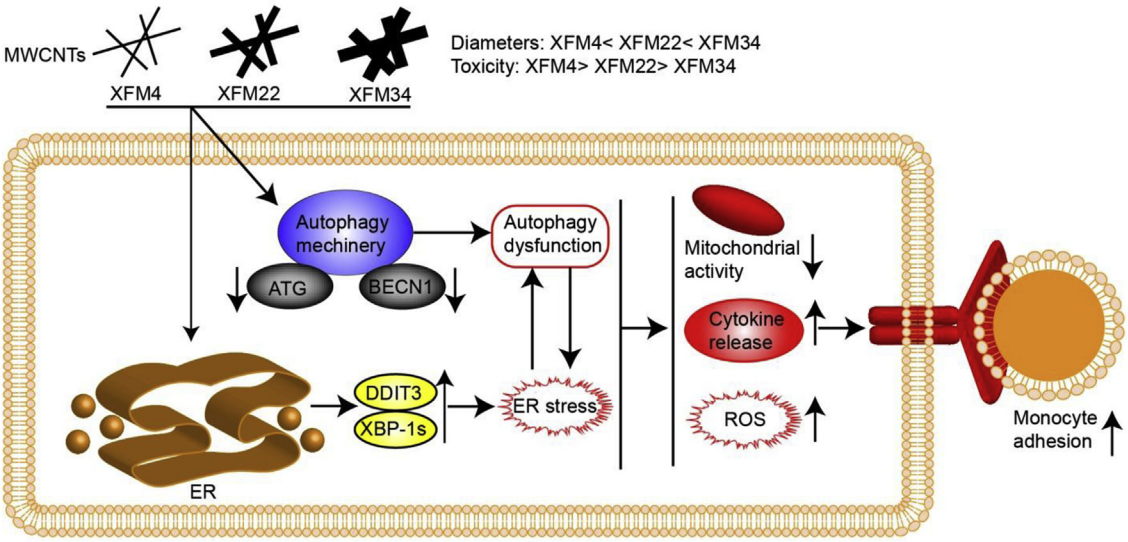

Fig. 10. The proposed mechanism of toxicity of MWCNTs to HUVECs. Exposure to MWCNTs may alter autophagy-ER stress pathway, consequently leading to toxicity in the form of decreased cellular viability, inflammatory responses, and oxidative stress. The toxicity of MWCNTs to HUVECs may decrease with an increase in the diameter of MWCNTs. See more in the text.

a mouse has a blood volume of 80 mL/kg. Su et al. injected mouse with 40 μg MWCNT-based nanocomplexes for cancer therapy, which corresponds to approximately 20 μg/mL MWCNTs in blood (Su et al., 2017). In nanotoxicology, Tang et al. found that mice administered with 100 μg MWCNTs (equals to 50 μg/mL in blood) showed no adverse effect (Tang et al., 2012). In contrast, Xu et al. showed that rats injected with 200 μg/kg MWCNTs (equals to about 4 μg/mL MWCNTs in blood, assuming a rat has a blood volume of 50 mL/kg) showed accelerated development of atherosclerosis (Xu et al., 2012). The concentrations used in this study might be reached *in vivo* in animal models after intravenous injection.

Taken together, the results of the present study revealed the diameter-dependent toxicity of MWCNTs to HUVECs. Based on the same mass concentration, the toxicity of MWCNTs could be decreased with an increase in the diameter of MWCNTs. As illustrated in Fig. 10, we suggest that the diameter-dependent toxicity of MWCNTs is associated with the interconnection between autophagy dysfunction and ER stress that could lead to decreased mitochondrial activity, oxidative stress, and inflammatory responses. The results from this study may provide important information for the rational design of MWCNTs that are biocompatible with the vascular system.

Competing interests

No.

Appendix A. Supplementary data

Supplementary data to this article can be found online at https://doi.org/10.1016/j.fct.2019.02.026.

Transparency document

Transparency document related to this article can be found online at https://doi.org/10.1016/j.fct.2019.02.026

Funding

This work was financially supported by the National Natural Science Foundation of China (Grant No. 21707114).

References

Bhattacharjee, S., 2016. DLS and zeta potential - what they are and what they are not? J. Contr. Release 235, 337–351.
Cao, Y., Gong, Y., Liu, L., Zhou, Y., Fang, X., Zhang, C., Li, Y., Li, J., 2017a. The use of human umbilical vein endothelial cells (HUVECs) as an in vitro model to assess the toxicity of nanoparticles to endothelium: a review. J. Appl. Toxicol. 37, 1359–1369.
Cao, Y., Jacobsen, N.R., Danielsen, P.H., Lenz, A.G., Stoeger, T., Loft, S., Wallin, H., Roursgaard, M., Mikkelsen, L., Moller, P., 2014. Vascular effects of multiwalled carbon nanotubes in dyslipidemic ApoE-/- mice and cultured endothelial cells. Toxicol. Sci. 138, 104–116.
Cao, Y., Long, J., Liu, L., He, T., Jiang, L., Zhao, C., Li, Z., 2017b. A review of endoplasmic reticulum (ER) stress and nanoparticle (NP) exposure. Life Sci. 186, 33–42.
Chang, S., Zhao, X., Li, S., Liao, T., Long, J., Yu, Z., Cao, Y., 2018. Cytotoxicity, cytokine release and ER stress-autophagy gene expression in endothelial cells and alveolar-endothelial co-culture exposed to pristine and carboxylated multi-walled carbon nanotubes. Ecotoxicol. Environ. Saf. 161, 569–577.
Cohignac, V., Landry, M.J., Ridoux, A., Pinault, M., Annangi, B., Gerdil, A., Herlin-Boime, N., Mayne, M., Haruta, M., Codogno, P., Boczkowski, J., Pairon, J.C., Lanone, S., 2018. Carbon nanotubes, but not spherical nanoparticles, block autophagy by a shape-related targeting of lysosomes in murine macrophages. Autophagy 14, 1323–1334.
Eom, H.J., Roca, C.P., Roh, J.Y., Chatterjee, N., Jeong, J.S., Shim, I., Kim, H.M., Kim, P.J., Choi, K., Giralt, F., Choi, J., 2015. A systems toxicology approach on the mechanism of uptake and toxicity of MWCNT in Caenorhabditis elegans. Chem. Biol. Interact. 239, 153–163.
Gao, J., Zhang, X., Yu, M., Ren, G., Yang, Z., 2015. Cognitive deficits induced by multi-walled carbon nanotubes via the autophagic pathway. Toxicology 337, 21–29.
Gorain, B., Choudhury, H., Pandey, M., Kesharwani, P., Abeer, M.M., Tekade, R.K., Hussain, Z., 2018. Carbon nanotube scaffolds as emerging nanoplatform for myocardial tissue regeneration: a review of recent developments and therapeutic implications. Biomed. Pharmacother. 104, 496–508.
Hamilton, R.F., Wu, Z., Mitra, S., Holian, A., 2018. The effects of varying degree of MWCNT carboxylation on bioactivity in various in vivo and in vitro exposure models. Int. J. Mol. Sci. 19, E354.
Kafa, H., Wang, J.T., Rubio, N., Klippstein, R., Costa, P.M., Hassan, H.A., Sosabowski, J.K., Bansal, S.S., Preston, J.E., Abbott, N.J., Al-Jamal, K.T., 2016. Translocation of LRP1 targeted carbon nanotubes of different diameters across the blood-brain barrier in vitro and in vivo. J. Contr. Release 225, 217–229.
Li, Y., Cao, J., 2018. The impact of multi-walled carbon nanotubes (MWCNTs) on macrophages: contribution of MWCNT characteristics. Sci. China Life Sci. 61, 1333–1351.
Li, Y., Ju, D., 2018. The role of autophagy in nanoparticles-induced toxicity and its related cellular and molecular mechanisms. Adv. Exp. Med. Biol. 1048, 71–84.
Long, J., Xiao, Y., Liu, L., Cao, Y., 2017. The adverse vascular effects of multi-walled carbon nanotubes (MWCNTs) to human vein endothelial cells (HUVECs) in vitro: role of length of MWCNTs. J. Nanobiotechnol. 15, 80.
Louro, H., 2018. Relevance of physicochemical characterization of nanomaterials for understanding nano-cellular interactions. Adv. Exp. Med. Biol. 1048, 123–142.
Lu, N., Sui, Y., Tian, R., Peng, Y.Y., 2018. Adsorption of plasma proteins on single-walled carbon nanotubes reduced cytotoxicity and modulated neutrophil activation. Chem. Res. Toxicol. 31, 1061–1068.
Mocan, T., Matea, C.T., Pop, T., Mosteanu, O., Buzoianu, A.D., Suciu, S., Puia, C., Zdrehus, C., Iancu, C., Mocan, L., 2017. Carbon nanotubes as anti-bacterial agents.

Cell. Mol. Life Sci. 74, 3467–3479.
Moller, P., Christophersen, D.V., Jacobsen, N.R., Skovmand, A., Gouveia, A.C., Andersen, M.H., Kermanizadeh, A., Jensen, D.M., Danielsen, P.H., Roursgaard, M., Jantzen, K., Loft, S., 2016. Atherosclerosis and vasomotor dysfunction in arteries of animals after exposure to combustion-derived particulate matter or nanomaterials. Crit. Rev. Toxicol. 46, 437–476.
Orecna, M., De Paoli, S.H., Janouskova, O., Tegegn, T.Z., Filipova, M., Bonevich, J.E., Holada, K., Simak, J., 2014. Toxicity of carboxylated carbon nanotubes in endothelial cells is attenuated by stimulation of the autophagic flux with the release of nanomaterial in autophagic vesicles. Nanomedicine 10, 939–948.
Ou, L., Song, B., Liang, H., Liu, J., Feng, X., Deng, B., Sun, T., Shao, L., 2016. Toxicity of graphene-family nanoparticles: a general review of the origins and mechanisms. Part. Fibre Toxicol. 13, 57.
Park, E.J., Zahari, N.E., Kang, M.S., Lee, S., Lee, K., Lee, B.S., Yoon, C., Cho, M.H., Kim, Y., Kim, J.H., 2014. Toxic response of HIPCO single-walled carbon nanotubes in mice and RAW264.7 macrophage cells. Toxicol. Lett. 229, 167–177.
Poulsen, S.S., Jackson, P., Kling, K., Knudsen, K.B., Skaug, V., Kyjovska, Z.O., Thomsen, B.L., Clausen, P.A., Atluri, R., Berthing, T., Bengtson, S., Wolff, H., Jensen, K.A., Wallin, H., Vogel, U., 2016. Multi-walled carbon nanotube physicochemical properties predict pulmonary inflammation and genotoxicity. Nanotoxicology 10, 1263–1275.
Raffa, V., Ciofani, G., Vittorio, O., Riggio, C., Cuschieri, A., 2010. Physicochemical properties affecting cellular uptake of carbon nanotubes. Nanomedicine (Lond). 5, 89–97.
Rashid, H.O., Yadav, R.K., Kim, H.R., Chae, H.J., 2015. ER stress: autophagy induction, inhibition and selection. Autophagy 11, 1956–1977.
Rezaee, M., Behnam, B., Banach, M., Sahebkar, A., 2018. The Yin and Yang of carbon nanomaterials in atherosclerosis. Biotechnol. Adv. 36, 2232–2247.
Saleem, J., Wang, L., Chen, C., 2018. Carbon-based nanomaterials for cancer therapy via targeting tumor microenvironment. Adv. Healthc. Mater., e1800525.
Setyawati, M.I., Tay, C.Y., Docter, D., Stauber, R.H., Leong, D.T., 2015. Understanding and exploiting nanoparticles' intimacy with the blood vessel and blood. Chem. Soc. Rev. 44, 8174–8199.
Smith, M., Wilkinson, S., 2017. ER homeostasis and autophagy. Essays Biochem. 61, 625–635.
Su, Y., Hu, Y., Wang, Y., Xu, X., Yuan, Y., Li, Y., Wang, Z., Chen, K., Zhang, F., Ding, X., Li, M., Zhou, J., Liu, Y., Wang, W., 2017. A precision-guided MWNT mediated reawakening the sunk synergy in RAS for anti-angiogenesis lung cancer therapy. Biomaterials 139, 75–90.
Suzuki, Y., Tada-Oikawa, S., Hayashi, Y., Izuoka, K., Kataoka, M., Ichikawa, S., Wu, W., Zong, C., Ichihara, G., Ichihara, S., 2016. Single- and double-walled carbon nanotubes enhance atherosclerogenesis by promoting monocyte adhesion to endothelial cells and endothelial progenitor cell dysfunction. Part. Fibre Toxicol. 13, 54.
Tang, S., Tang, Y., Zhong, L., Murat, K., Asan, G., Yu, J., Jian, R., Wang, C., Zhou, P., 2012. Short- and long-term toxicities of multi-walled carbon nanotubes in vivo and in vitro. J. Appl. Toxicol. 32, 900–912.
Tsukahara, T., Matsuda, Y., Haniu, H., 2014. The role of autophagy as a mechanism of toxicity induced by multi-walled carbon nanotubes in human lung cells. Int. J. Mol. Sci. 16, 40–48.
Vance, M.E., Kuiken, T., Vejerano, E.P., McGinnis, S.P., Hochella Jr., M.F., Rejeski, D., Hull, M.S., 2015. Nanotechnology in the real world: redeveloping the nanomaterial consumer products inventory. Beilstein J. Nanotechnol. 6, 1769–1780.
Wang, J.T., Rubio, N., Kafa, H., Venturelli, E., Fabbro, C., Menard-Moyon, C., Da, R.T., Sosabowski, J.K., Lawson, A.D., Robinson, M.K., Prato, M., Bianco, A., Festy, F., Preston, J.E., Kostarelos, K., Al-Jamal, K.T., 2016. Kinetics of functionalised carbon nanotube distribution in mouse brain after systemic injection: spatial to ultra-structural analyses. J. Contr. Release 224, 22–32.
Wu, L., Zhang, Y., Zhang, C., Cui, X., Zhai, S., Liu, Y., Li, C., Zhu, H., Qu, G., Jiang, G., Yan, B., 2014. Tuning cell autophagy by diversifying carbon nanotube surface chemistry. ACS Nano 8, 2087–2099.
Xu, Y.Y., Yang, J., Shen, T., Zhou, F., Xia, Y., Fu, J.Y., Meng, J., Zhang, J., Zheng, Y.F., Yang, J., Xu, L.H., Zhu, X.Q., 2012. Intravenous administration of multi-walled carbon nanotubes affects the formation of atherosclerosis in Sprague-Dawley rats. J. Occup. Health 54, 361–369.
Yang, F., Jiang, Q., Xie, W., Zhang, Y., 2017. Effects of multi-walled carbon nanotubes with various diameters on bacterial cellular membranes: cytotoxicity and adaptive mechanisms. Chemosphere 185, 162–170.
Zhao, M., Cao, Y., Liu, X., Deng, J., Li, D., Gu, H., 2014. Effect of nitrogen atomic percentage on N+-bombarded MWCNTs in cytocompatibility and hemocompatibility. Nanoscale Res. Lett. 9, 142–149.
Zhao, C., Zhou, Y., Liu, L., Long, J., Liu, H., Li, J., Cao, Y., 2018. Lipid accumulation in multi-walled carbon nanotube-exposed HepG2 cells: possible role of lipophagy pathway. Food Chem. Toxicol. 121, 65–71.